Bioactive Materials 26 (2023) 249–263

Contents lists available at ScienceDirect

Bioactive Materials

journal homepage: www.keaipublishing.com/en/journals/bioactive-materials

Fibroblast exosomal TFAP2C induced by chitosan oligosaccharides promotes peripheral axon regeneration via the miR-132-5p/CAMKK1 axis

Yahong Zhao [a], Jina Liu [a], Sha Liu [a], Panpan Yang [b], Yunyun Liang [a], Jinyu Ma [a], Susu Mao [a], Cheng Sun [a,**], Yumin Yang [a,*]

[a] Key Laboratory of Neuroregeneration of Jiangsu Province and Ministry of Education, Co-Innovation Center of Neuroregeneration, NMPA Key Laboratory for Research and Evaluation of Tissue Engineering Technology Products, Nantong University, 19 Qixiu Road, Nantong, Jiangsu, 226001, China
[b] School of Medicine, Nantong University, 19 Qixiu Road, Nantong, Jiangsu, 226001, China

ARTICLE INFO

Keywords:
peripheral nerves
chitosan oligosaccharides
fibroblast exosomes
TFAP2C
axon regeneration

ABSTRACT

Chitosan and its degradation product, oligosaccharides, have been shown to facilitate peripheral nerve regeneration. However, the underlying mechanisms are not well understood. In this study, we analyzed the protein expression profiles in sciatic nerves after injury using proteomics. A group of proteins related to exosome packaging and transport is up-regulated by chitosan oligosaccharides (COS), implying that exosomes are involved in COS-induced peripheral nerve regeneration. In fact, exosomes derived from fibroblasts (f-EXOs) treated with COS significantly promoted axon extension and regeneration. Exosomal protein identification and functional studies, revealed that TFAP2C is a key factor in neurite outgrowth induced by COS-f-EXOs. Furthermore, we showed that TFAP2C targets the pri-miRNA-132 gene and represses miR-132-5p expression in dorsal root ganglion neurons. *Camkk1* is a downstream substrate of miR-132-5p that positively affects axon extension. In rats, miR-132-5p antagomir stimulates CAMKK1 expression and improves axon regeneration and functional recovery in sciatic nerves after injury. Our data reveal the mechanism for COS in axon regeneration, that is COS induce fibroblasts to produce TFAP2C-enriched EXOs, which are then transferred into axons to promote axon regeneration via miR-132-5p/CAMKK1. Moreover, these results show a new facet of fibroblasts in axon regeneration in peripheral nerves.

1. Introduction

Unlike axon regeneration in the central nervous system (CNS), axon regeneration in the peripheral nervous system (PNS) is relatively easy and achievable [1–3]. However, long distance defects in the PNS remain a challenge at clinics [4]. Autologous nerve implantation exhibits the best outcomes and is considered as the gold standard of surgical intervention for peripheral axon regeneration [5]. However, limited sources and permanent injuries at the donor sites significantly impede wide application of this technique. Therefore, artificial grafts are used at the center of peripheral nerve surgery [6,7].

Artificial grafts made of natural and/or synthetic biopolymers that are designed to have the necessary mechanical and biochemical cues for neural regeneration. There has been numerous of studies reported on various fronts (design, materials, preparation methods, factors, etc.) to achieve the onerous task of getting an ideal artificial graft [8,9]. The basic expectations of a material include biocompatibility, biodegradability, and appropriate mechanical properties. The physical, chemical, biochemical and topographical features regulate functional recovery of damaged peripheral nerves, which should be considered in the design of artificial grafts by different fabrication methods [10]. The advent of advanced technologies such as injection molding, 3D bioprinting, electrospining, have been employed for fabricating artificial grafts. Injection molding technique was used to fabricate artificial grafts with intraluminal channels. Different patterns of aligned and random fibrous regions can be generated by electrospining [11]. 3D bioprinting could be beneficial in easing the production of patient-specific artificial grafts [12]. Artificial grafts loaded with neurotropic factors, drugs and genes are some of the futuristic areas of interest since the sequence, timing, dosage, delivery vector, and duration of therapy remain to be solved [7].

Peer review under responsibility of KeAi Communications Co., Ltd.
* Corresponding author.
** Corresponding author.
E-mail addresses: suncheng1975@ntu.edu.cn (C. Sun), yangym@ntu.edu.cn (Y. Yang).

https://doi.org/10.1016/j.bioactmat.2023.03.002
Received 2 January 2023; Received in revised form 3 March 2023; Accepted 3 March 2023

Chitosan is a naturally derived polysaccharide with distinguished biocompatibility, bio degradation, and antimicrobial properties [13]. Hence chitosan itself and its derivatives are widely employed for diverse biomedical applications such as food processing, water treatment, cosmetics, and fabrics [14]. It has been shown that chitosan-based nerve grafts achieve great successes in peripheral nerve regeneration in various animals including rats, dogs, and monkeys [15–18]. Notably, the nerve scaffolds constructed by chitosan exhibit excellent performances in clinical trials [19]. Recently, one chitosan-based nerve graft was developed by our group, which received a certificate of pharmaceutical product from the National Medical Products Administration in China (approval number, 20203130898). In addition to being a conduit for connecting injured nerves, scaffold degradation products, chitosan oligosaccharides (COS), are vital to peripheral nerve regeneration. For example, COS stimulate Schwann cell proliferation and thus promote sciatic nerve regeneration [20]. Moreover, by constructing a favorable microenvironment at the injury site, COS facilitate peripheral nerve regeneration after injury in rats [21]. Axon regeneration is a key event in peripheral nerve regeneration [1]. However, COS and axon regeneration in peripheral nerves have not been investigated sufficiently.

Exosomes are nanometer-sized vesicles secreted by cells under both normal and pathophysiological settings [22]. Exosomes contain various biological molecules such as proteins, lipids, and nucleic acids, which endow them with essential roles in cellular communications [23]. Numerous studies have shown that exosomes are involved in the progression of various diseases including cancer, diabetes, osteoporosis, atherosclerosis, and neurodegeneration associated disorders [24–28]. Exosomes from healthy tissues or stem cells facilitate the treatment of the diseases as mentioned above [29–33]. Engineered or regulatable exosomes with specific cargo and target molecules may offer significant therapeutic potentials [34].

Therefore, in the present study, we performed a series of experiments to determine the effects of COS on axonal growth and regeneration in peripheral nerves. Our data showed that fibroblast derived exosomes (f-EXOs) are key in axon extension and regeneration after injury. COS treatment could reinforce TFAP2C expression in EXOs produced from fibroblasts, which are then transferred into axons and facilitated axon growth by targeting the miR-132-5p/CAMKK1 axis.

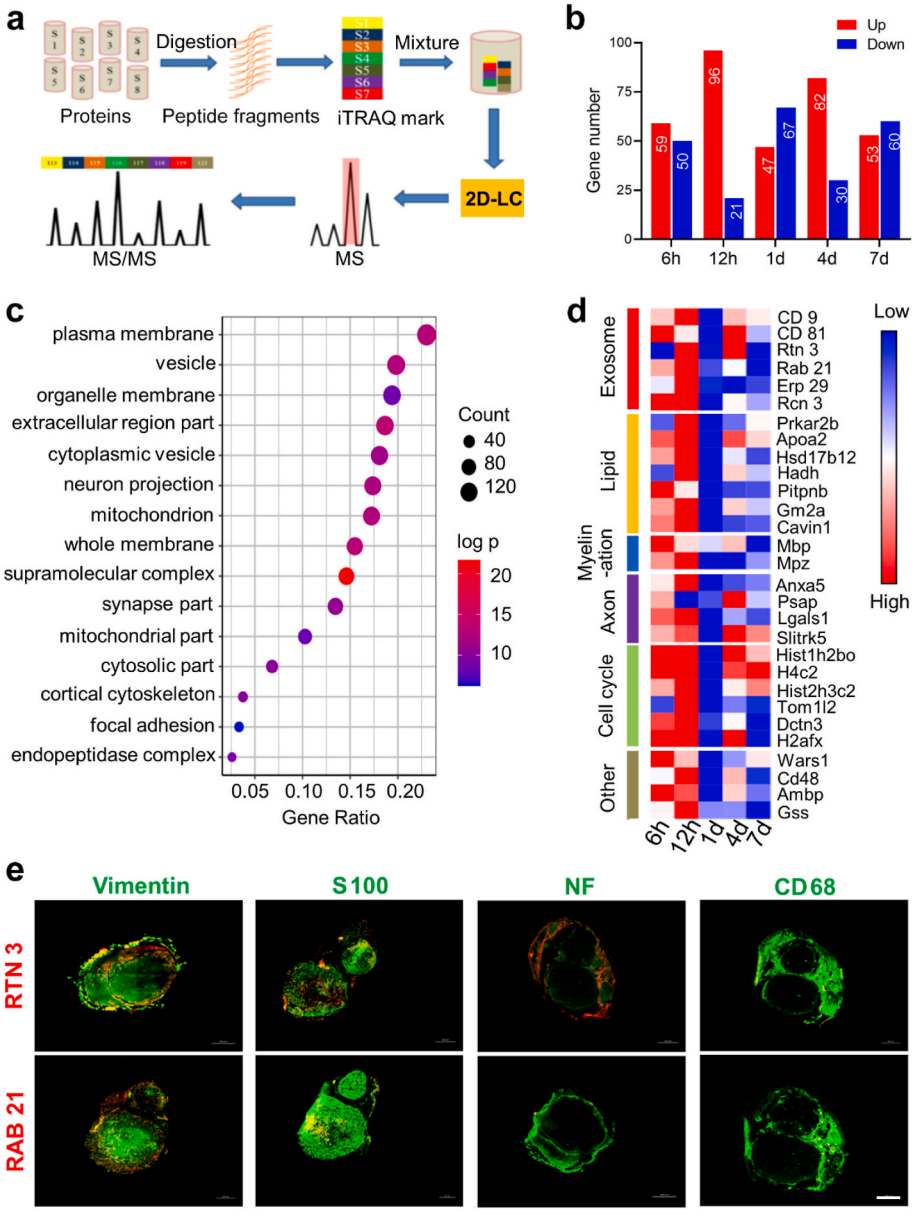

Fig. 1. Fibroblasts derived exosomes are involved in COS-induced axon elongation.
a The workflow for iTRAQ analysis of sciatic nerve samples from rats. 10-mm sciatic nerve defects were bridged with COS- or saline-filled silicone tubes. The proximal regenerated nerves at lesion sites were harvested at 6 h, 12 h, 1 d, 4 d, and 7 d post-surgery (n = 3). The samples were resolved by SDS-PAGE, followed by trypsin digestion and iTRAQ labeling, and then subjected to strong cation exchange fractionation and LC-MS/MS analysis.**b** The number of differentially expressed proteins ($p < 0.05$) induced by COS at different time points.**c** Significant Gene Ontology analysis of differentially expressed proteins induced by COS. The dot size represents functional significance. Gene number represents the number of proteins in each term. Red is a strong positive correlation, and blue is a strong negative correlation. **d** Heatmap showing relative expression patterns of proteins with selected enriched cluster terms.**e** Immunofluorescence staining for Vimentin, S100, NF, CD68, RTN3, and RAB21 in the cross sections of sciatic nerves at 4 days post-bridging with silicon tubes. Scar bar = 200 μm.

2. Results

2.1. Identification of differentially expressed proteins in sciatic nerves induced by COS

Chitosan degradation products such as COS have been shown to facilitate peripheral nerve regeneration after injury [20]. To reveal the underlying mechanisms, 10 mm defects in rat sciatic nerves were constructed and bridged with silicone tubes filled with COS. The sciatic nerves were harvested at 6 h, 12 h, 1 d, 4 d and 7 d post-surgery and used for protein sample preparation, subsequently, they were subjected to proteomic analysis using isobaric tags for relative and absolute quantification (iTRAQ) (Fig. 1a). The resulting mass data were processed using a common pipeline to obtain 2049 total quantified proteins. Differentially expressed proteins were identified based on the following criteria: $P < 0.05$ and at least 1.5-fold changes (Table S1). Using these criteria, 337 up-regulated and 228 down-regulated proteins were induced by COS across all the time points (Fig. 1b). Cellular component analysis showed that these differentially expressed proteins are closely related to vesicle formation, transport, budding or endocytosis, which are evident in components such as plasma membrane, vesicle, organelle membrane, cytoplasmic vesicle, whole membrane, focal adhesion, and mitochondrion (Fig. 1c). The heatmap further indicated that exosome-related proteins such as CD9, CD81, RAB21, ERP29 and RTN3 were increased at the early stages (Fig. 1d). Other clusters, including lipid, myelination, axon and the cell cycle are pivotal events in nerve regeneration [35,36]. These data strongly implied that exosome-related biological events are involved in COS-induced improved peripheral nerve regeneration after injury. Fibroblasts, Schwann cells, axon and macrophages are the main components at the injured sites of sciatic nerves [35]. To determine the cells that contribute to exosome secretion, therefore, we performed immunofluorescence analysis using antibodies against RTN3 or RAB21 (exosome-related proteins), Vimentin (fibroblast marker), S100 (Schwann cell marker), NF (axon marker), or CD68 (macrophage marker). The results showed that both RTN3 and RAB21 were colocalized with Vimentin positive cells (Fig. 1e). No obvious overlapping signals were observed between RTN3/RAB21 and S100/NF/CD68 (Fig. 1e). These evidences suggest that exosomes mainly derived from fibroblasts (f-EXOs), which are responsible for COS-induced sciatic regeneration after injury. In fact, f-EXOs have been shown to promote Schwann cell myelination in peripheral nerves [37].

2.2. Exosomes derived from COS-treated fibroblasts promote neurite outgrowth in vitro

Our above data indicate that f-EXOs might contribute significantly to

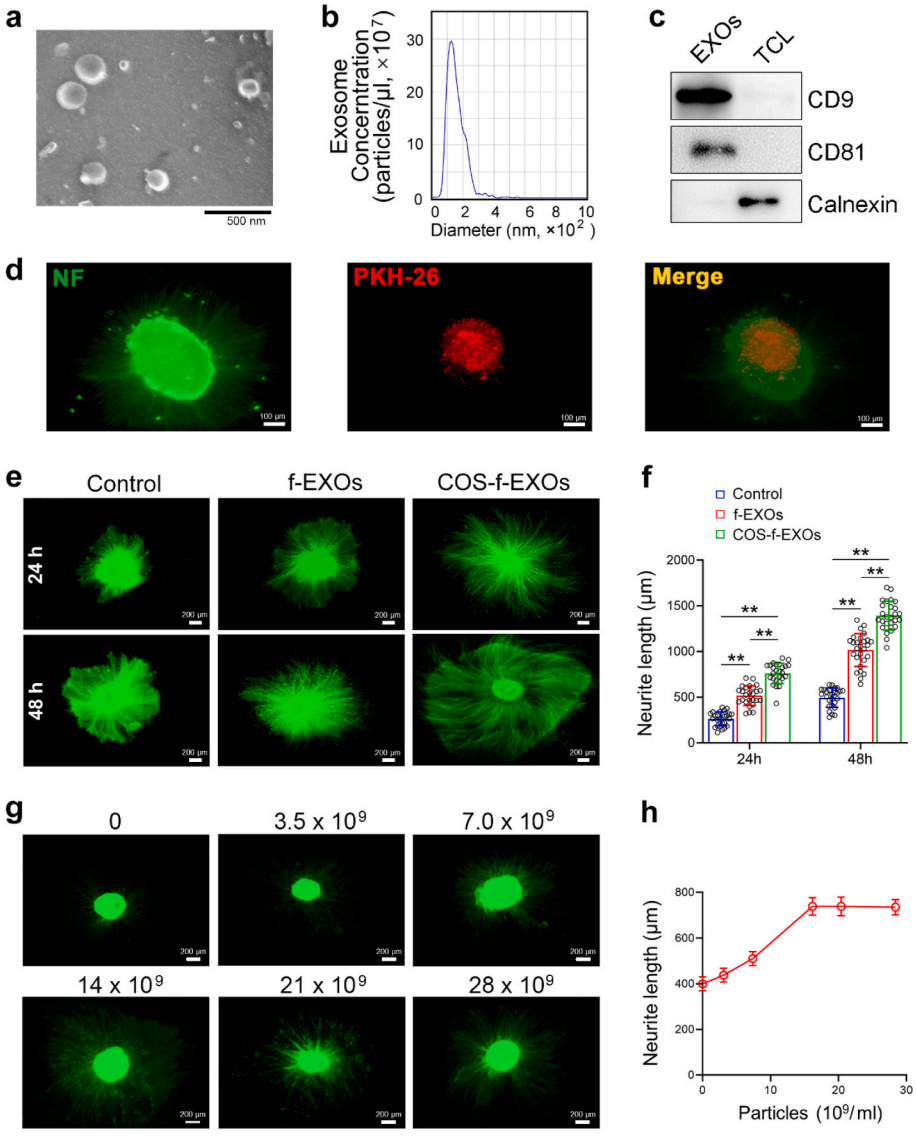

Fig. 2. Exosomes derived from COS-treated fibroblasts facilitate neurite outgrowth.
a Transmission Electron Microscopy (TEM) analysis of exosomes secreted by fibroblasts. Scale bar = 500 nm **b** Particle size distribution of the vesicles secreted from fibroblasts was measured by Nanoparticle Tracking Analysis (NTA).**c** Exosome markers CD9 and CD81 were analyzed by western blot. Calnexin was used as a negative control. EXOs: exosomes; TCL: total cell lysates.**d** Fluorescent microscopy analysis showing fibroblasts derived exosomes were internalized by cultured DRG neurons. Exosomes derived from fibroblasts were labeled by PKH26 (red) and co-cultured with DRG neurons for 24 h, then DRG neurons were subjected to immunofluorescence analysis using an anti-NF antibody (green). Scale bar = 100 μm.**e** Neurite outgrowth was stimulated by exosomes from COS-treated fibroblasts. Exosomes from fibroblasts (f-EXOs) treated with or without COS were prepared and co-cultured with DRG neurons for 24 h or 48 h. The neurite outgrowth was evaluated by immunofluorescence analysis by using an anti-NF antibody. Scale bar = 200 μm.**f** Quantification of neurite length as shown in (**e**). n = 8.**g** Exosomes derived from COS-treated fibroblasts promote neurite outgrowth. DRG neurons were incubated with exosomes at different concentrations as indicated for 24 h. Neurite outgrowth was measured by immunofluorescence analysis by using an anti-NF antibody. Scale bar = 200 μm **h** Quantification of neurite length as shown in (**g**). n = 8.Error bar represents ±SD. $^{**}P < 0.01$, two-way ANOVA analysis.

nerve regeneration induced by COS. Therefore, we next isolated f-EXOs and examined their effects on neurite growth. Transmission electron microscopy images showed that the prepared f-EXOs exhibited a cup-like shape (Fig. 2a). The diameters of the f-EXOs are mainly ranged from 50 to 150 nm (Fig. 2b). Exosomal markers such as CD9 and CD81 were presented in the isolated f-EXOs (Fig. 2c). The immunofluorescence data showing f-EXOs (PKH-26; red) could be internalized by dorsal root ganglion (DRG) neurons (Fig. 2d). This exosome internalization in DRG neurons was gradually increased along with time elongation (Fig. S1). All these features confirmed that the prepared extracellular vesicles are exosomes [22]. Next, we examined the effects of f-EXOs on neurite outgrowth. As shown in Fig. 2e, the neurite outgrowth was markedly promoted by f-EXOs and EXOs from COS-treated fibroblasts (COS-f-EXOs). Notably, compared with f-EXOs, COS-f-EXOs further fortified neurite outgrowth (Fig. 2e and f). Moreover, this promotion occurred in a dose-dependent manner within the ranges from 0 to 14 x 10^9 exosome particles/ml; subsequently, the promotion on neurite outgrowth stabilized (Fig. 2g and h). In addition, the treatment of COS increased cell viability and proliferation in primary fibroblasts (Figs. S2a–c). However, COS had no effect on exosome characteristics (Figs. S3a and b). These results clearly indicate that f-EXOs, especially COS-f-EXOs, can stimulate neurite outgrowth *in vitro*.

2.3. COS-f-EXOs improve axon regeneration in sciatic nerves after injury

To evaluate the potential effects of COS-f-EXOs on axon growth *in vivo*, 10-mm long defects in rat sciatic nerves were bridged with silicone tubes filled with f-EXOs or COS-f-EXOs. In comparison with the control group, the elongation of amputated axons was promoted by f-EXOs, particularly by COS-f-EXOs, at the 14th day after surgery (Fig. 3a and b). Moreover, results of walking track analysis showed that both the intensity and contact area of the left hind (LH) paws were reduced significantly after injury compared with those of the uninjured right hind (RH) paws (Fig. 3c). The application of f-EXOs and COS-f-EXOs attenuated these reductions in terms of intensity and contact area (Fig. 3d and e). Notably, compared with f-EXOs, COS-f-EXOs exhibited better performances in terms of axon regeneration and in the walking track analysis. Together, these *in vitro* and *in vivo* functional studies strongly suggest that f-EXOs are the main executor for translating the beneficial roles of COS in peripheral nerve regeneration.

2.4. Exosomal TFAP2C is a key factor for neurite outgrowth

Next, we attempted to identify the constituents in the COS-f-EXOs that contribute to the observed benefits for axon growth. Hence, we prepared protein samples from EXOs and analyzed them by mass spectrometry. In total, 673 proteins were identified, among which 237 proteins were defined as differentially expressed proteins in COS-f-EXOs (Table S2). Of these differentially expressed proteins, 130 proteins were downregulated and 107 proteins were upregulated (Table S2). Functional annotation showed that these upregulated proteins are closely related with axon growth as evidenced by modules of neuron projection, axon, and neurofilament (Fig. 4a). More importantly, most of the proteins in these modules were increased in the COS-f-EXOs (Fig. 4b). We focused on protein TFAP2C, as it is a master transcriptional factor with pleiotropic roles in various cellular events including maintaining stem

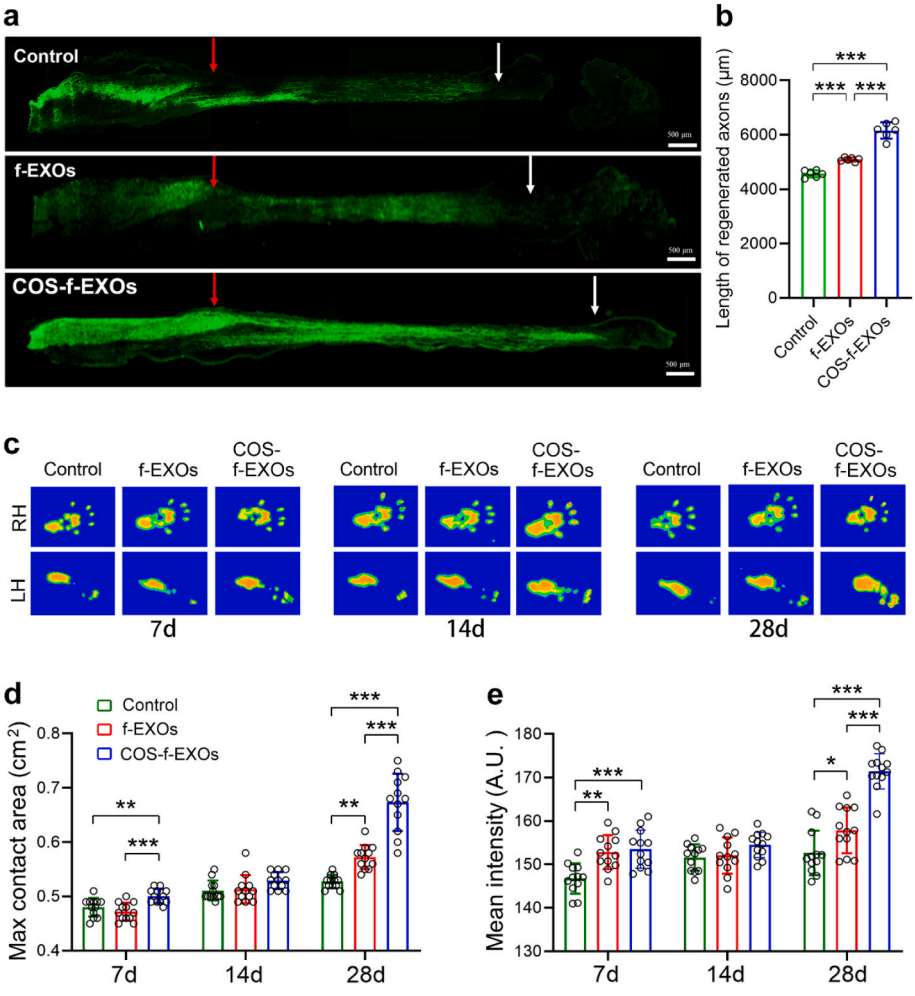

Fig. 3. Exosomes derived from COS-treated fibroblasts promote axon regeneration and functional recovery in rats with injured sciatic nerves.
a Axon regeneration in sciatic nerves was promoted by exosomes from COS-treated fibroblasts (COS-f-EXOs). The transected sciatic nerves were bridged with silicone tubes filled with saline, f-EXOs, or COS-f-EXOs. 14 days post-surgery, the proximal nerve stumps were subjected to immunofluorescence analysis by using an anti-NF antibody. Red arrows indicate the start sites of axon regeneration, and white arrows indicate the axon growth cones. Scale bar = 500 μm **b** The length of regenerated axons as shown in (**a**). n = 5.**c** Walking track analysis showing COS-f-EXOs promote functional recovery in rats with injured sciatic nerves. RH means right hind paw. LH means left hind paw. n = 6.**d-e** The maximum contact mean area (**d**) and the mean intensity (**e**) were measured according to the walking track data.Error bar represents ± SD.*$P < 0.05$, **$P < 0.01$, ***$P < 0.001$, one-way ANOVA test (b) and two-way ANOVA test (d, e).

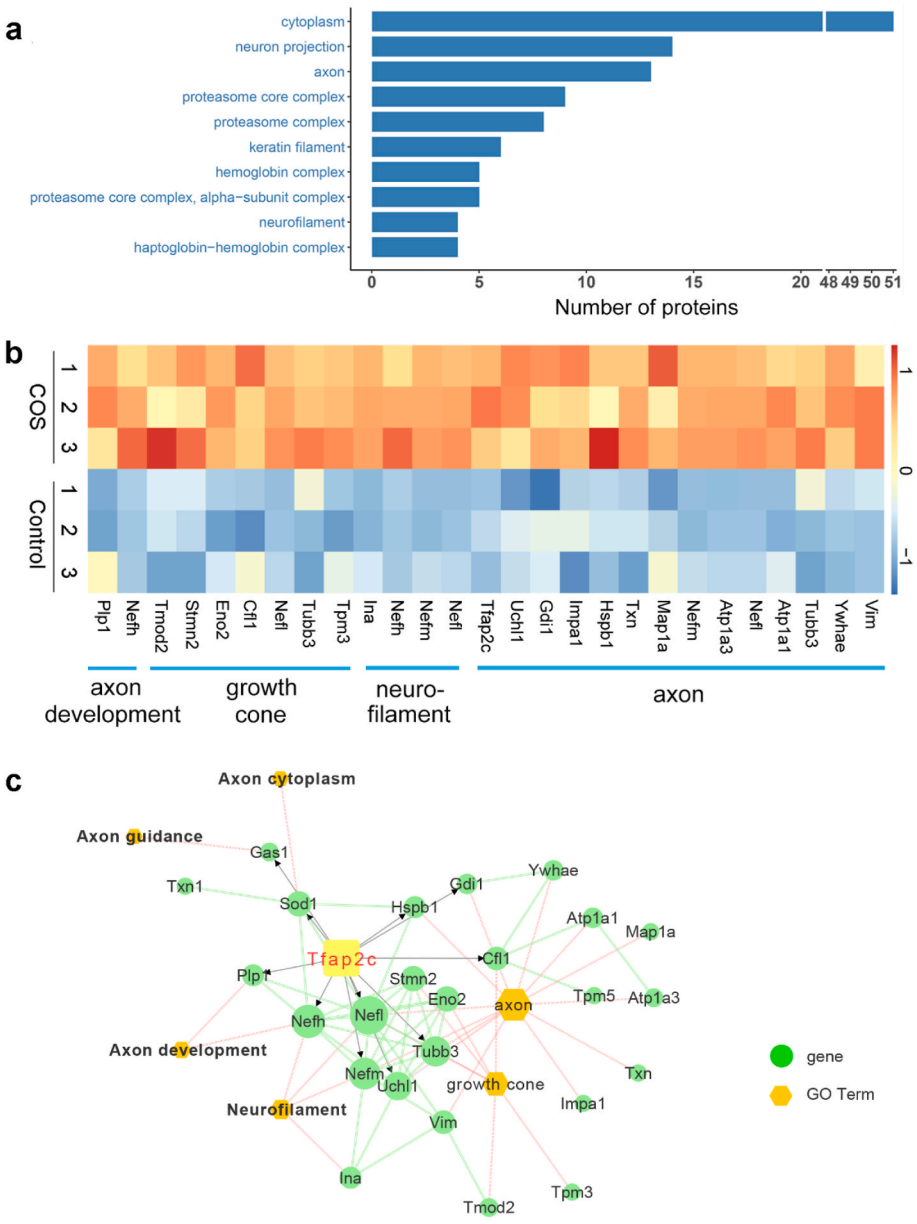

Fig. 4. Exosomal protein identification.
Proteins were isolated from exosomes and subjected to mass spectrometry analysis. The up-regulated proteins enriched in exosomes from COS-treated fibroblasts were further analyzed by bioinformatics analysis. Differentially expressed proteins were defined as $P < 0.05$ with at least 1.2-fold changes. **a** Cellular components. **b** Heat map and functional annotations. **c** Network analysis for *Tfap2c*.

cell pluripotency [38], germline formation [39], carcinogenesis [40], keratinocyte development [41], cell collision guidance [42], estrogen receptor-driven cell proliferation [43], and embryo polarization [44]. Results from bioinformatics analysis revealed that TFAP2C might be involved in axon cytoplasm, axon guidance and development, and neurofilament (Fig. 4c), suggesting that TFAP2C may be a strong candidate for promoting axon regeneration. To verify this prediction, we transfected DRG neurons with a plasmid expressing *Tfap2c* by electroporation and discovered that this treatment markedly induced neurite outgrowth (Fig. 5a). Furthermore, we downregulated *Tfap2c* expression using siRNAs in DRG neurons (Fig. 5b and c). Knockdown *Tfap2c* by siRNA2 largely repressed neurite outgrowth (Fig. 5d). To further confirm the critical role of TFAP2C in axon growth, we also manipulated *Tfap2c* expression in fibroblasts to alter its expression in EXOs. As shown in Fig. 5e, the exosomal TFAP2C was increased in EXOs prepared from fibroblasts transfected with the plasmid of *Tfap2c*. As expected, the neurite outgrowth was enhanced owing to TFAP2C-enriched EXOs (Fig. 5f). Moreover, TFAP2C-deficient EXOs were prepared from siRNA2-transfected fibroblasts (Fig. 5g). Using these engineered EXOs to treat DRG neurons reduced neurite outgrowth (Fig. 5h). These data clearly indicate that exosomal TFAP2C from fibroblasts is crucial in transducing the benefits in axon regeneration induced by COS. In line with our findings, TFAP2C has been shown to be crucial in inducing adult hippocampal glutamatergic neurogenesis in mice [45].

2.5. TFAP2C targets miR-132-5p for inducing neurite outgrowth

Next, we investigated the downstream effectors of TFAP2C in neurite growth. First, we analyzed the potential promoters with binding capacity with TFAP2C, since the latter is a transcriptional factor [38,39]. Motifs such as 5′-GCCN$_3$GGC-3′, 5′-GCCN$_4$GGC-3′, 5′-GCCN$_{3/4}$GGG-3′, and 5′-CCCCAGGC-3′ have been shown to be promising binding sites for TFAP2C [46]. We blasted these motifs with the genome and focused on one gene for pri-miRNA-132 because its promoter contains all known binding sites for TFAP2C. In addition, we noticed that the gene for encoding pri-miRNA-132 was an intergenic miRNA located in chromosome 10 (Fig. 6a). To examine whether TFAP2C affects the expression of pri-miRNA-132, we constructed four plasmids, in which luciferase was

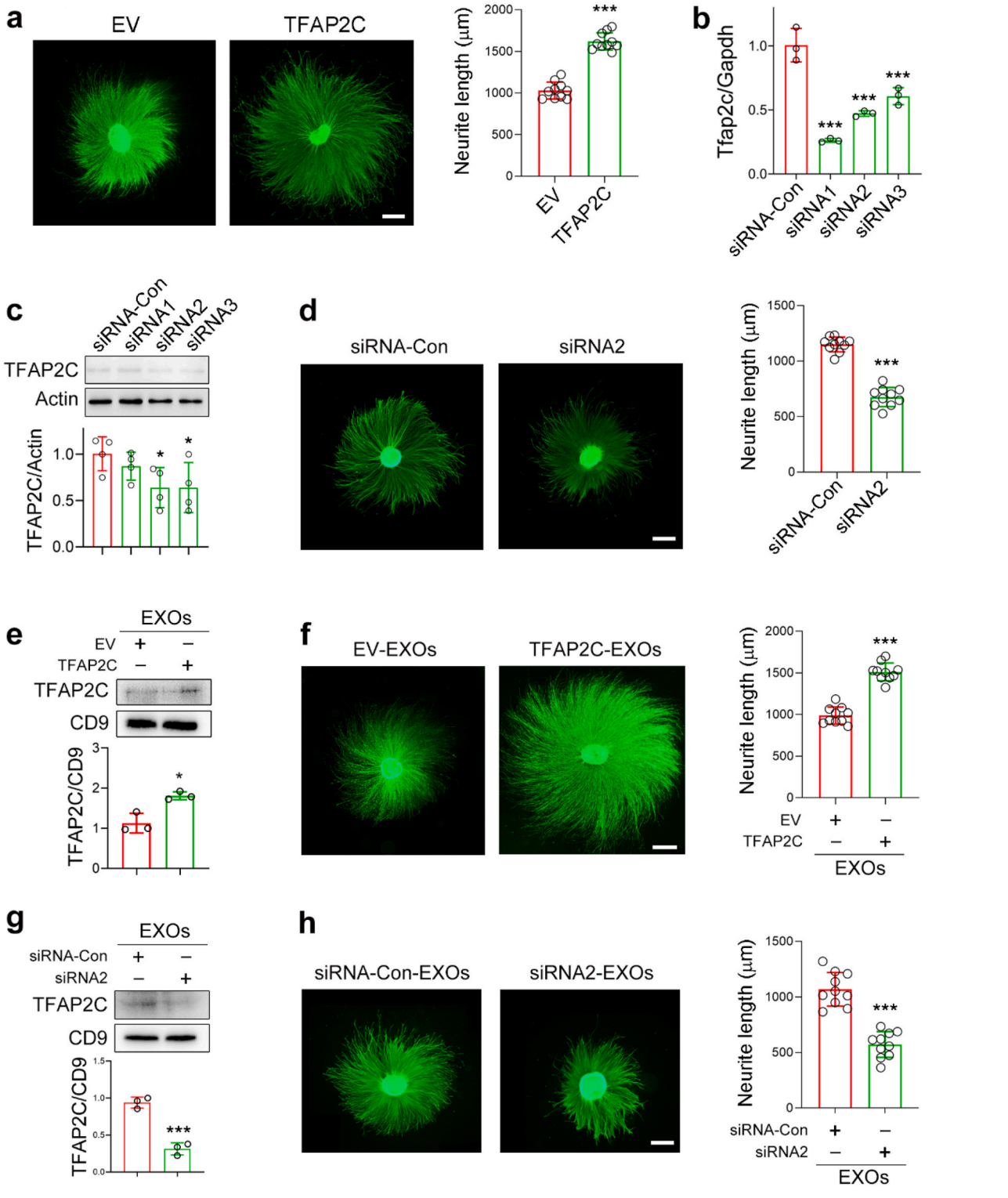

(caption on next page)

Fig. 5. TFAP2C is a positive regulator for neurite outgrowth.
a TFAP2C induces neurite outgrowth. Cultured DRG neurons were transfected with the plasmid expressing *Tfap2c* by electroporation. 24 h post-transfection, neurons were subjected to immunofluorescence analysis using an anti-NF antibody. Scale bar = 500 μm. n = 8.**b-c** Knockdown of *Tfap2c*. Cultured DRG neurons were transfected with siRNA-Con, or siRNA-1, or -2, or -3 by electroporation. 48 h post-transfection, neurons were harvested for gene expression analysis by qRT-PCR (b) or western blot (c). *Gapdh* was used as an internal control in qRT-PCR analysis, while Actin was used a loading control in western blot analysis. n = 3.**d** Knockdown of *Tfap2c* represses neurite outgrowth. Cultured DRG neurons were transfected with siRNA-2 by electroporation. 48 h post-transfection, DRG neurons were subjected to immunofluorescence analysis using an anti-NF antibody. Scale bar = 500 μm. n = 8.**e** Preparation of TFAP2C-enriched exosomes from fibroblasts. Primary fibroblasts were transfected with the plasmid expressing *Tfap2c* by electroporation. 48 h post-transfection, cell culture medium was collected for preparing exosomes. Exosomal TFAP2C was analyzed by western blot. CD9 was used as a loading control. n = 3.**f** TFAP2C-enriched exosomes stimulate neurite outgrowth. Cultured DRG neurons were treated with TFAP2C-enriched exosomes for 24 h, and neurite outgrowth was analyzed by immunofluorescence staining with an anti-NF antibody. Scale bar = 500 μm. n = 8.**g** Preparation of TFAP2C-deficient exosomes from fibroblasts. Primary fibroblasts were transfected with *Tfap2c* siRNA-2. 72 h post-transfection, cell culture medium was collected for preparing exosomes. Exosomal TFAP2C was analyzed by western blot. CD9 was used as a loading control. n = 3.**h** TFAP2C-deficient exosomes impede neurite outgrowth. Cultured DRG neurons were treated with TFAP2C-knockdown exosomes for 24 h, and neurite outgrowth was analyzed by immunofluorescence staining with an anti-NF antibody. Scale bar = 500 μm. n = 8.EV: empty vector. Error bar represents ±SD.*$P < 0.05$, ***$P < 0.001$, Student's *t*-test.

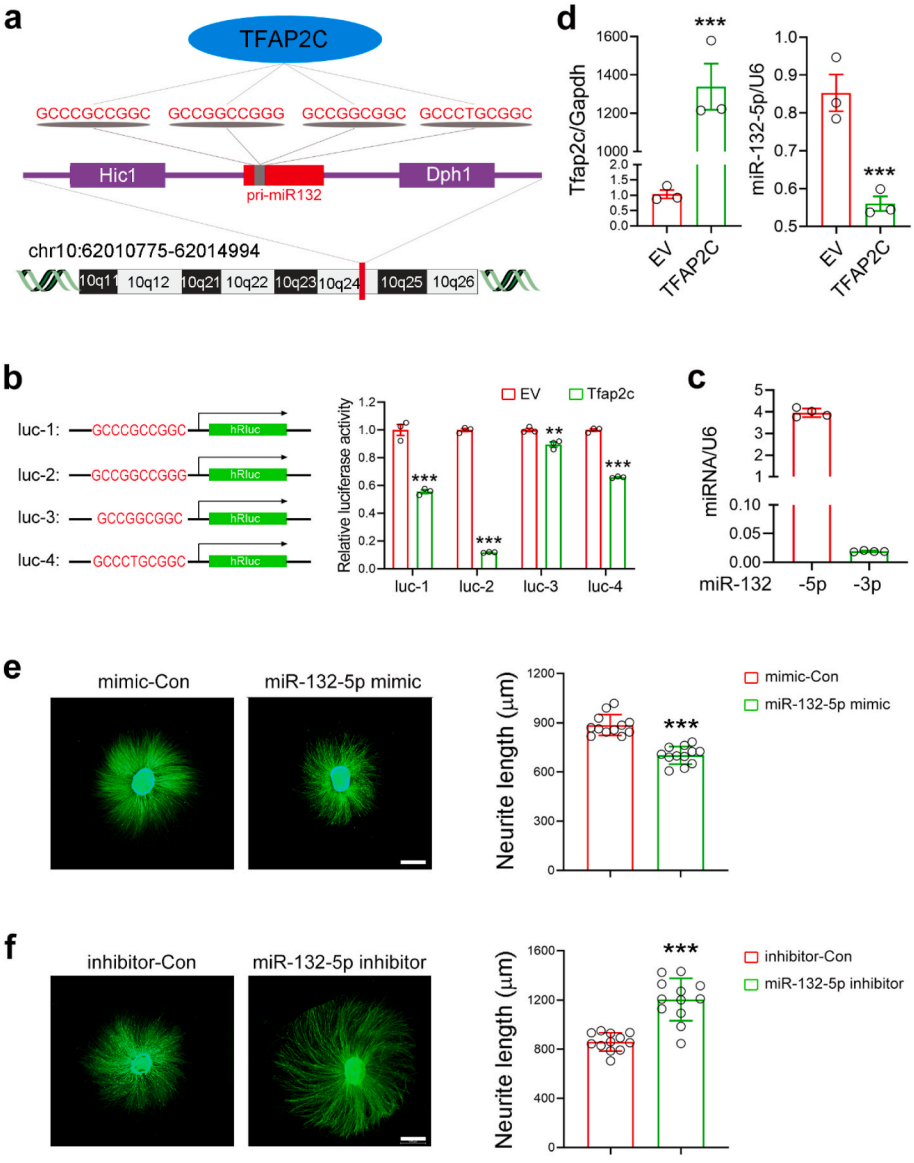

Fig. 6. TFAP2C targets miR-132-5p to regulate neurite extension.
a Identification of pri-miRNA-132 as a potential downstream effector of TFAP2C by bioinformatics analysis.**b** TFAP2C inhibits luciferase activity drove by the sequences in pri-miRNA-132 gene. 4 sequences containing TFAP2C binding sites were synthesized and incorporated into luciferase vector. 293T cells were co-transfected with the constructed luciferase plasmids and the plasmid expressing *Tfap2c*. 24 h post-transfection, cells were harvested for luciferase activity assay. EV: empty vector. n = 3.**c** The expression profiles of miR-132-3p and -5p in cultured DRG neurons. The expression of miRNA was analyzed by qRT-PCR, U6 was used as an internal control. n = 4.**d** Overexpression of TFAP2C represses miR-132-5p expression. Cultured DRG neurons were transfected with the plasmid expressing *Tfap2c* by electroporation. 24 h post-transfection, total RNA was extracted for analyzing the expression of *Tfap2c* and miR-132-5p by qRT-PCR. *Gapdh* and *U6* were used as internal controls. EV: empty vector. n = 3.**e-f** The effects of miR-132-5p on neurite outgrowth. Cultured DRG neurons were transfected with miR-132-5p mimic (**e**) or inhibitor (**f**) by electroporation. 24 h post-transfection, neurite outgrowth was analyzed by immunofluorescence using an anti-NF antibody. Scale bar = 500 μm. n = 8.Error bar represents ±SD. **$P < 0.01$, ***$P < 0.001$, Student's *t*-test.

driven by different sequences containing the bindings sites present in the up-stream region of the pri-miRNA-132 gene. As shown in Fig. 6b, luciferase activities were decreased by TFAP2C, with luc-2 being the most affected. Pri-miRNA-132 gene contains two products, miR-132-3p and miR-132-5p. To determine the miRNA that is the downstream substrate of TFAP2C, we first examined the expression profiles of the two abovementioned miRNAs in cultured DRG. The results showed that miR-132-5p is a predominant isoform in DRG neurons (Fig. 6c), hence, it was selected for further analysis. Next, we examined the direct effect of TFAP2C on miR-132-5p expression in axons. Cultured DRG neurons were transfected with a plasmid expressing *Tfap2c*. As expected, the expression of miR-132-5p was decreased significantly due to TFAP2C

(Fig. 6d). Next, we examined whether miR-132-5p affects axon growth. In this regard, we transfected cultured DRG neurons with a miR-132-5p mimic or inhibitor. As shown in Fig. 6e, the miR-132-5p mimic repressed neurite outgrowth. By contrast, miR-132-5p inhibitor stimulated neurite outgrowth (Fig. 6f). These data indicate that TFAP2C targets and represses miR-132-5p in DRG neurons to facilitate neurite outgrowth.

2.6. *miR-132-5p downregulates CAMKK1 expression to repress neurite growth*

In most cases, miRNAs perform their biological functions by suppressing their target genes. To identify the substrate of miR-132-5p, we performed bioinformatics analysis using the Target Scan software (Fig. 7a). Among the predicted substrates, we focused on one gene, i.e., *Camkk1*, as its homolog *Camkk2* has been shown to contribute significantly to cerebellar granule cell development [47], which suggest that

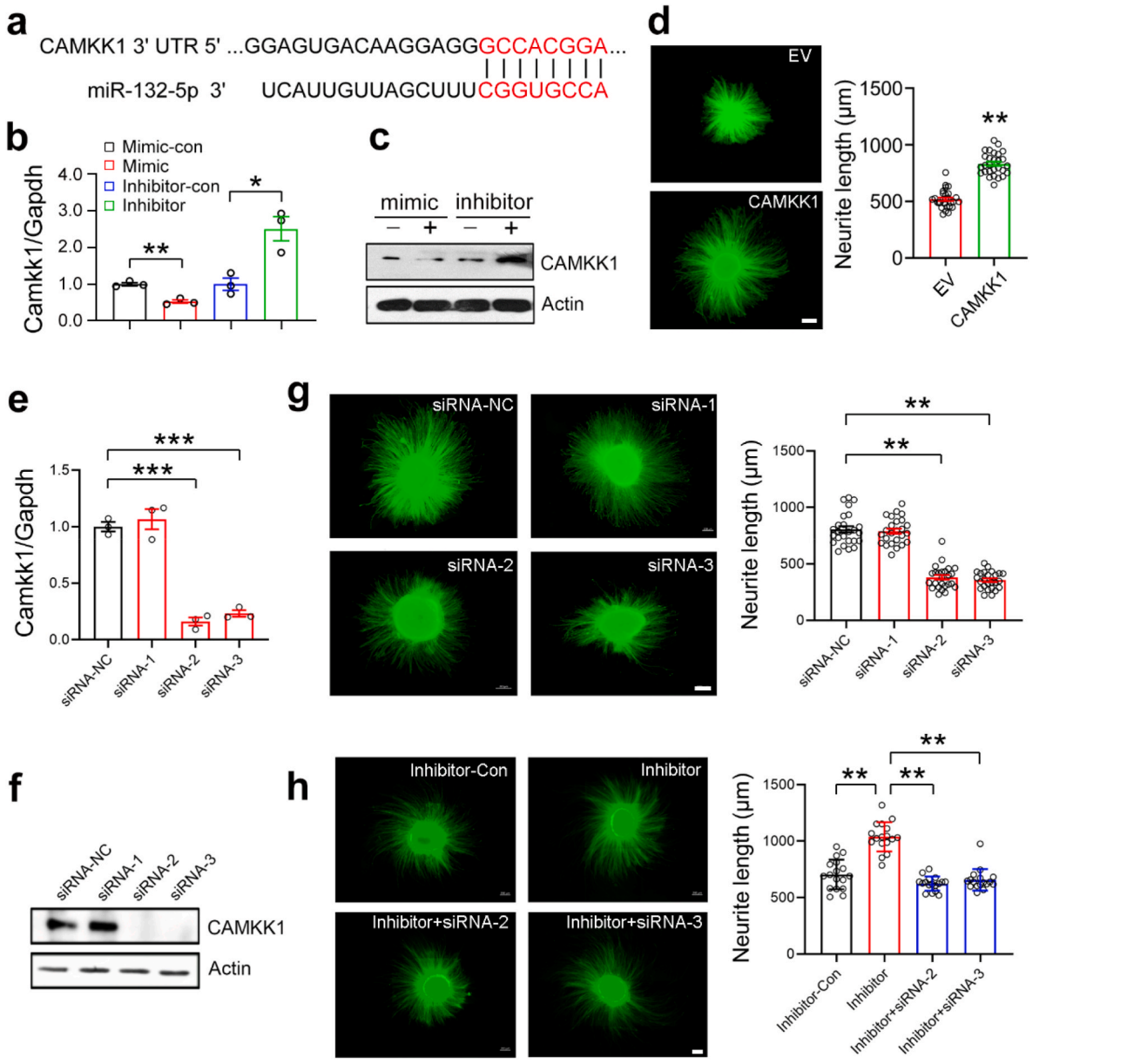

Fig. 7. *Camkk1* is a substrate of miR-132-5p for its repression on neurite outgrowth.
a Bioinformatics analysis showing miR-132-5p interacts with the 3′-untranslated region (UTR) of *Camkk1*.**b-c** The effects of miR-132-5p on *Camkk1* expression. Cultured DRG neurons were transfected with miR-132-5p mimic or inhibitor by electroporation. 36 h post-transfection, *Camkk1* expression was analyzed by qRT-PCR (**b**) or western blot (**c**). *Gapdh* was used as an internal control. Actin was used as a loading control. n = 3.**d** CAMKK1 stimulates neurite outgrowth. Cultured DRG neurons were transfected with the plasmid expressing *Camkk1* by electroporation. 24 h post-transfection, the neurite length was analyzed by immunostaining for NF. Scale bar = 200 μm. n = 8.**e-f** *Camkk1* knockdown. DRG neurons were transfected with the *Camkk1* siRNAs by electroporation. 48 h post-transfection, the mRNA levels and the protein levels of *Camkk1* were analyzed by qRT-PCR (**e**) and western blot (**f**), respectively. *Gapdh* was used as an internal control in qRT-PCR analysis and Actin was used as a loading control in western blot analysis.**g** *Camkk1* knockdown retards neurite outgrowth. DRG neurons were transfected with the *Camkk1* siRNAs by electroporation. 36 h post-transfection, the neurite outgrowth was analyzed by immunostaining for NF. Scale bar = 200 μm. n = 8.**h** *Camkk1* knockdown abolishes miR-132-5p inhibitor induced neurite outgrowth. DRG neurons were transfected with miR-132-5p inhibitor and *Camkk1* siRNAs as indicated by electroporation. 36 h post-transfection, the neurite length was evaluated by immunostaining for NF. Scale bar = 200 μm. n = 8.Data are expressed as means ± SD. $^{**}P < 0.01$, $^{**}P < 0.001$, Student's *t*-test was used to analyze statistical difference in (**b**, **d**, **e**, **g**). One-way ANOVA was used to analyze statistical difference in (**h**).

Camkk1 might participate in neurogenesis such as neurite extension. In this regard, we first analyzed whether *Camkk1* was targeted by miR-132-5p. In cultured DRG neurons, we found that the miR-132-5p mimic repressed the expression of *Camkk1*, whereas the miR-132-5p inhibitor enhanced *Camkk1* expression at both the mRNA and protein levels (Fig. 7b and c). Next, we examined the effects of CAMKK1 on neurite outgrowth. The transfection of CAMKK1 in cultured DRG neurons markedly increased neurite length (Fig. 7d). Using siRNA-mediated gene knockdown, CAMKK1 expression was successfully reduced by siRNA-2 and -3, whereas siRNA-1 failed to alter the expression of CAMKK1 (Fig. 7e and f). Functional studies showed that the neurite length was decreased by *Camkk1* siRNA-2 and -3, but not by siRNA-1 (Fig. 7g). Moreover, the increased neurite outgrowth by the miR-132-5p inhibitor can be mitigated by the knockdown of *Camkk1* (Fig. 7h). These data clearly indicate that miR-132-5p targets *Camkk1* to impede neurite outgrowth in the DRG neurons.

2.7. Inhibition of miR-132-5p improves axon regeneration

In the following experiments, we analyzed the *in vivo* effects of miR-132-5p on axonal growth. To this end, we used a rat model with a 10-mm long sciatic nerve defect. The defects were bridged with silicone tubes, in which miR-132-5p antagomir or negative control was infused. Fourteen days post-surgery, the injured nerves were harvested for further analysis. The expression of miR-132-5p was decreased in sciatic nerves treated with the antagomir (Fig. 8a). Accordingly, the expression of CAMKK1 was increased owing to the antagomir (Fig. 8b and c). The immunofluorescence data showed that axon regeneration in sciatic nerves was improved by the antagomir (Fig. 8d). Results of walking track analysis revealed that the locomotor function in rats treated with the antagomir was fortified as evidenced by the enhanced sciatic function index (SFI) (Fig. 8e). Results of electrophysiological analysis showed that the motor nerve conduction velocity in sciatic nerves was increased by the antagomir, although the compound muscle action potential (CMAP) amplitude was not altered (Fig. 8f–h). These data further confirmed that the miR-132-5p/CAMKK1 axis plays a key role in axon regeneration after injury. To reinforce this conclusion, we analyzed the *in vivo* effects of COS-f-EXOs on the expressions of miR-132-5p and CAMKK1. The results showed that the expression of miR-132-5p was repressed by COS-f-EXOs, whereas CAMKK1 was stimulated (Fig. 9a–c). The Akt pathway is a downstream target of CAMKK1, and its activation is considered as a positive signal for growth. Therefore, we analyzed this

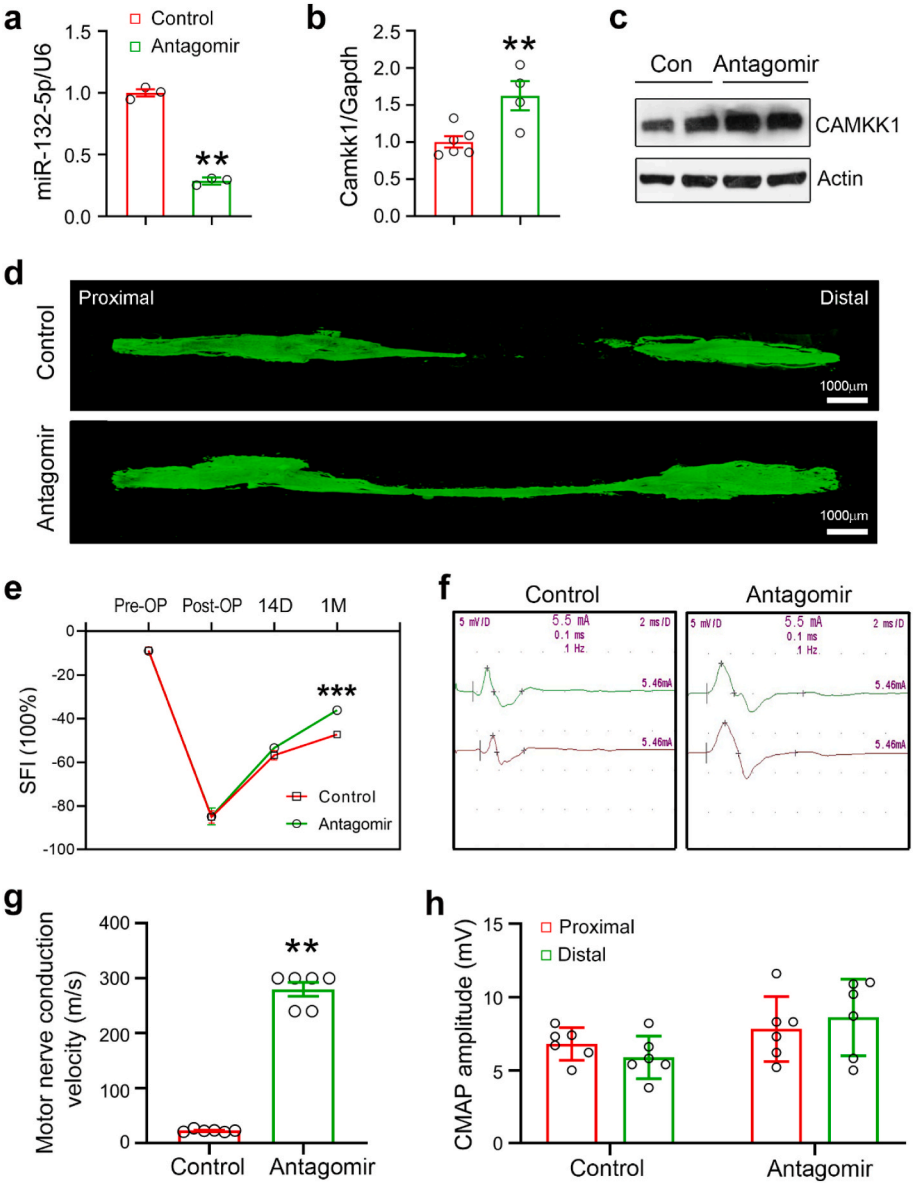

Fig. 8. Inhibition of miR-132-5p promotes sciatic nerve functional recovery after injury.
10-mm sciatic nerve defects were constructed in rats and bridged with silicone tubes filled with miR-132-5p antagomir or control.**a** The expression of miR-132-5p in sciatic nerves was reduced by miR-132-5p antagomir. qRT-PCR was used to analyze miR-132-5p expression and U6 was used as an internal control. n = 3.**b-c** The expression of *Camkk1* in sciatic nerves was increased by miR-132-5p antagomir. *Camkk1* expression was analyzed by qRT-PCR (**b**; n = 4–6) or western blot (**c**; n = 3). *Gapdh* was used as an internal control in qRT-PCR, Actin was used as a loading control in western blot.**d** miR-132-5p antagomir promotes axon regeneration in sciatic nerves after injury. Sciatic nerves were harvested at 14 d post-surgery and subjected to immunofluorescence analysis by using an anti-NF antibody. Scale bar = 1000 μm.**e** Sciatic functional index (SFI) calculated from the walking track analysis at different time-points after surgery. 14D and 1 M mean 14 days, and 1 month, respectively. n = 6.**f-h** Electrophysiological assay in sciatic nerves. The assay was carried out at 4 weeks post-surgery and the representative recordings were shown in (**f**). The motor nerve conduction velocity (**g**) in sciatic nerves and the compound muscle action potential (CMAP) recordings (**h**) were detected in the injured side of animals. n = 6.Data are expressed as means ± SD. $^{**}P < 0.01$, $^{***}P < 0.001$, Student's *t*-test.

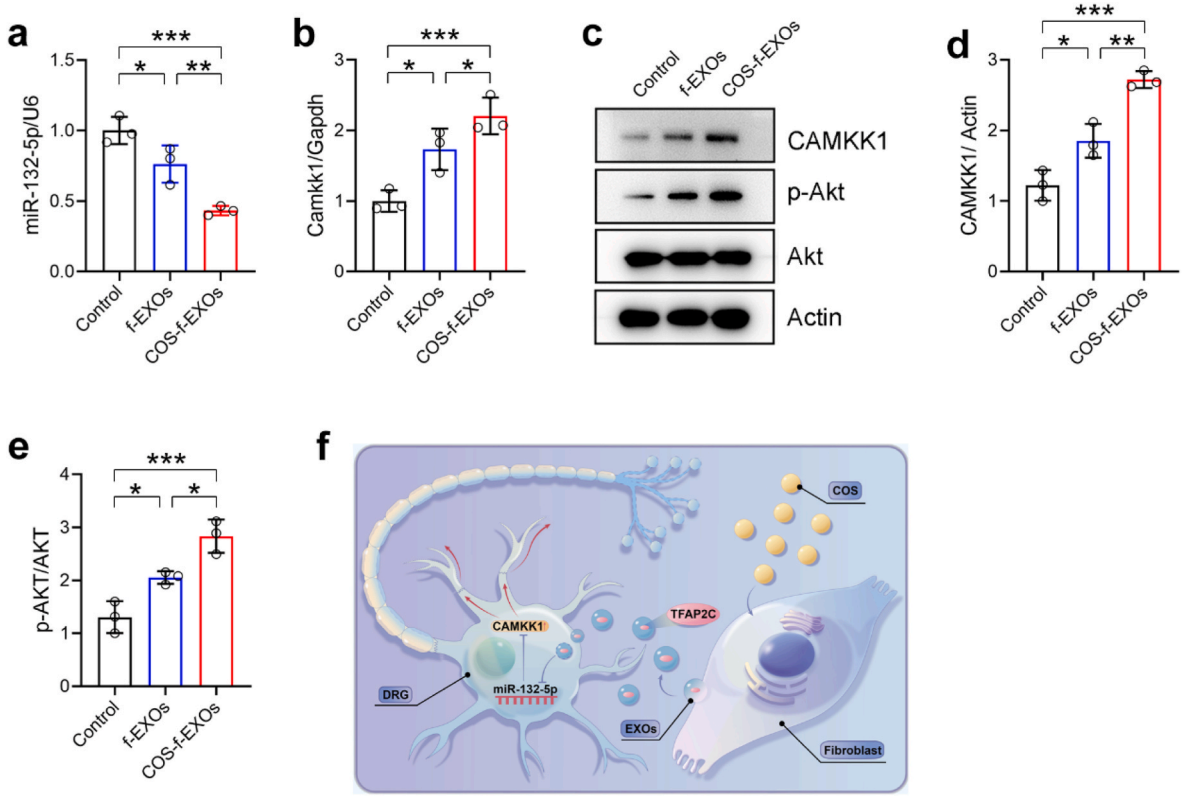

Fig. 9. The *in vivo* effects of f-EXOs and COS-f-EXOs on the expressions of miR-132-5p and CAMKK1.
Transected sciatic nerves were bridged with silicone tubes filled with saline, f-EXOs, or COS-f-EXOs. 7 days post-surgery, the proximal nerve stumps were collected for further analysis.**a** COS-f-EXOs repress the expression of miR-132-5p. qRT-PCR was used to analyze miR-132-5p expression and U6 was used as an internal control. n = 3.**b** COS-f-EXOs stimulate the expression of *Camkk1*. *Camkk1* expression was analyzed by qRT-PCR and *Gapdh* was used as an internal control. n = 3.**c** COS-f-EXOs increase CAMKK1 expression and phosphorylated Akt (p-Akt). Proteins were analyzed by western blot and Actin was used as a loading control. n = 3.**d-e** Quantification of CAMKK1 (**d**) and p-Akt (**e**). n = 3.**f** Schematic model for elucidating the molecular mechanism of COS-f-EXOs induced neurite outgrowth.Data are expressed as means ± SD. $^{*}P < 0.05$, $^{**}P < 0.01$, $^{***}P < 0.001$, one-way ANOVA.

pathway and found that phosphorylated Akt (p-Akt) was enhanced by COS-f-EXOs (Fig. 9c–e). The proposed working model was illustrated in Fig. 9f.

3. Discussion

In the present study, we aimed to investigate the mechanisms involved in COS, a degradative product of chitosan, which induced axon regeneration in peripheral nerves after injury. Our data showed that COS targets fibroblasts to produce TFAP-2C enriched exosomes, which are then transferred into axons and promote axon growth. In detail, TFAP-2C binds to the promoter region of the pre-miR-132 gene, thus reducing the expression of miR-132-5p. Consequently, *Cammk1* expression was stimulated because it is a substrate gene of miR-132-5p. Eventually, increased expression of *Cammk1* promotes axon growth in the sciatic nerves. By this way, COS play a beneficial role in axon regeneration in peripheral nerves.

Chitosan is a deacetylated derivative of chitin, which is an abundant natural biopolymer comprising of b-1,4-linked glucosamine moieties. Chitosan has been widely used in the pharmaceutical and biomedical fields due to its biodegradable, nontoxic, antimicrobial, and hemostatic properties [13,14]. In our laboratory, we developed a chitosan-constructed nerve graft to bridge transected peripheral nerves, which has achieved significant success in clinical trials. Consequently, it was approved by the National Medical Products Administration in China with the reference number of 20203130898. During the research and development stage of this nerve graft, we found that it not only functioned as a tunnel for guiding axon regeneration [16,19,48], but also its degradation products, i.e., COS, favored axon regrowth and Schwann cell proliferation in peripheral nerves after injury [20,21,49]. Because axon regeneration is a pivotal event in nerve repair [35], we investigated the mechanism by which COS promote axon regrowth in this process. To this end, we performed proteomic analysis using injured sciatic nerves and found that several proteins related to exosome formation, secretion, and transport were upregulated by COS, indicating that exosomes might mediate the transduction of the benefits of COS during axon regrowth. Immunofluorescence data revealed that these exosome-related proteins were highly expressed in fibroblasts. Notably, fibroblasts are the main type of cells in peripheral nerves, which constitute 25% of the total composition [50]. However, information regarding the role of cells in the function of sciatic nerves is scarce. Studies have been shown that fibroblasts are vital to wound healing [51,52], tissue repair [53], scar formation [54], and tumor metastasis [55], although their main task is to synthesize and organize matrix proteins [56]. We previously showed that fibroblasts derived exosomes promoted Schwann cell-mediated peripheral neuron myelination [37]. In the present study, we similarly found that COS may target fibroblasts to induce axon regrowth, which involves exosomes. Our evidence further supports this notion, that is, fibroblasts derived exosomes can promote neurite outgrowth, particularly when fibroblasts are treated with COS.

Exosomes are nano-sized vesicles with a diameter measuring 30–150 nm and are secreted by the most types of cells via exocytosis [26]. Exosomes contain different bioactive molecules such as proteins, lipid, nucleic acids, and glycoconjugates [22]. By transporting these molecules into other cells, exosomes are considered as a transfer cargo for mediating cell-to-cell communications [22,26]. To identify the molecule(s) in exosomes that transduce the benefits of COS on neurite outgrowth, we compared the protein expression profiles between f-EXOs and

COS-f-EXOs via proteomic analysis. Among the up-regulated proteins in COS-f-EXOs, we focused on one protein TFAP2C, owing to its pleiotropic biological functions [38–40,45,46]. Both gain-of-function and loss-of-function studies confirmed that TFAP2C positively affects neurite growth. As a transcriptional factor, TFAP2C generally stimulates downstream gene expression after binding with specific motifs in the promoter [57]. However, in the present study, we found that TFAP2C represses the pri-miRNA-132 gene, which might be due to TFAP2C competitively interacting with some specific sites in the upstream region of pri-miRNA-132 gene, thus impeding the binding of other factors to induce the gene expression. In fact, TFAP2C has been characterized as a negative regulator of *CDKN1A* [58]. Moreover, TFAP2A has been shown to negatively regulate the expression of several genes, including *MCAM/MUC18*, *c/EBP-α* and *c-myc* [59,60]. Additionally, exosomal miRNAs may also play a role in the observed neurite outgrowth. Exosomal miR-20b-5p derived from hypothermia-treated microglia has been shown to promote neurite outgrowth and synapse recovery after traumatic brain injury [61]. Likewise, it has been shown that miR-133b in multipotent mesenchymal stromal cells produced exosomes stimulates neurite outgrowth [62].

CAMKK1 is a Ca^{2+}/calmodulin-dependent protein kinase belonging to the serine/threonine protein kinase family. CAMK1, CAMK1D, CAMK1G, and CAMK4, as substrates of CAMKK1, have been shown to be phosphorylated by CAMKK1. In the present study, we observed that CAMKK1 stimulates neurite outgrowth in DRG neurons, whereas the knockdown of *CAMKK1* represses neurite extension. To date, direct evidence to support the positive effects of CAMKK1 on neurite growth is not available. However, several lines of indirect evidence showed that CAMKK1 may have such a potential. For instance, CAMK1, a substrate of CAMKK1, has been shown to stimulate neurite elongation and growth cone motility [63]. Furthermore, in that study, the treatment of neurons with STO-609, which is an inhibitor of CAMKK, was shown to reduce neurite elongation and growth cone motility; notably, these inhibitory effects can be reversed by transfection with constitutively active CAMK1 [63]. Moreover, CAMK1 has been shown to promote neurite outgrowth by phosphorylating MARK2 on novel sites within its kinase domain [64]. Loss of CAMK1α markedly impairs the terminal axonal extension and thereby perturbs the projections from the interhemispheric callosal into the contralateral cortices [65]. In addition to CAMK1, CAMK4 was considered as a positive regulator of neurite outgrowth and dendrite elongation [66,67]. The abovementioned findings further support our conclusion that CAMKK1 promotes neurite outgrowth in DRG neurons.

In summary, our data revealed the underlying mechanisms for COS-promoted axon regeneration, i.e., COS targets fibroblasts in sciatic nerves and induces TFAP2C-enriched exosome secretion, thereby transferring TFAP2C into recipient axons, where TFAP2C down-regulates miR-132-5p to relieve its repression on *CAMKK1*, thus resulting in upregulated CAMKK1. Finally, increased expression of CAMKK1 promotes neurite outgrowth and thus facilitates axon regeneration in the peripheral nerves. These data provide insights into axon regeneration by defining the crosstalk between axon regrowth and fibroblasts. Moreover, our data also provide a theoretical basis for the clinical application of chitosan-based biomaterials in regenerative medicine.

4. Methods

4.1. Animal surgery and tissue preparation

The experiments were performed on adult male Sprague-Dawley (SD) rats weighing 180–220 g. The procedures for animal surgery and sciatic nerve tissue preparation were described previously [21]. Briefly, animals were anaesthetized by an intraperitoneal injection of 3% sodium pentobarbital solution (30 mg/kg). The sciatic nerves were exposed by making a skin incision and splitting the underlying muscles in left lateral thighs. Segments of sciatic nerves were resected and removed, leaving a 10-mm long defect following retraction of the nerve ends. The nerve defects were bridged with silicone tubes filled with 50 μl of 0.12 mg/ml COS or saline. To inhibit miR-132-5p *in vivo*, the transected sciatic nerves were bridged with silicone tubes filled with the miR-132-5p antagomir or control at the dosage of 5 nmol/rat. 6 rats were included in each group. After the implants were sutured to the proximal and distal nerve stumps, surgical incisions were closed in a routine fashion. All rats were housed and fed routinely, and euthanized at different time points. The regenerated nerves were collected for further immunochemical or biochemical analysis. All the animal protocols were approved by the Animal Care and Use Committee of Nantong University and the Jiangsu Province Animal Care Ethics Committee (Approval ID: SYXK (SU) 2017-0046), and the methods were carried out in accordance with the approved guidelines.

4.2. iTRAQ and bioinformatics analysis

After surgery, 8 mm-length sciatic nerves at proximal ends were collected for preparing protein samples. 3 rats were included at each time point (0, 6 h, 12 h, 1 d, 4 d and 7 d). The normal (unlesioned) nerve sample that was collected as control. The samples were processed by integrating trichloroacetic acid/acetone precipitation with phenol extraction [68]. Exosomes from fibroblasts treated with or without COS were prepared by ultracentrifugation. Exosomal proteins were extracted with a commercial kit from Invitrogen (Catalog No. 44-785-45). The prepared exosomal protein samples were subjected to proteomic analysis using iTRAQ at LuMing Biotech (Shanghai, China). iTRAQ proteomics was performed using an 8-plex procedure so that all experimental samples were processed in the same mass spectrometry (MS) run, together with the normal (unlesioned) nerve samples that were used as the baseline standards. Briefly, the proximal ends of regenerated nerves were harvested and subjected to SDS-PAGE. The resolved samples in gels were digested with trypsin solution at a ratio of protein: trypsin = 50 : 1 overnight to generate proteolytic peptides, which were then labeled with iTRAQ reagents. iTRAQ-labeled and trypsin digested peptide mixtures were then pooled and subjected to strong cation exchange (SCX) fractionation. The collected fractions were analyzed by liquid chromatography (LC) coupled with MS/MS (LC/MS/MS) analysis for both identification and quantification. The raw mass data were analyzed by the Proteome Discoverer 2.1 software (Thermo Fisher Scientific) based on the database connected to Uniprot website (http://www.uniprot.org/). The p value was calculated according to Student's *t*-test. P value was set as < 0.05 to identify proteins that were differentially expressed. To obtain an overview of the COS related proteomics, the differently expressed proteins were categorized based upon their expression profiles. Functional enrichment analysis was performed using Gene Ontology (GO) (http://www.geneontology.org/). Protein-protein interaction (PPI) networks are used for distinguishing hub genes, which are defined as genes with a high degree of connectivity that play an essential role in stabilizing the PPI network structure. PPI information was obtained from the STRING database; highest confidence of 0.900 was chosen (version 11.5, https://string-db.org/). The PPI networks for upregulated genes was constructed using Cytoscape software [69].

4.3. Preparation of primary fibroblasts

Fibroblasts were isolated from sciatic nerves of 1-day old Sprague Dawley (SD) rats with the method described elsewhere [37]. Briefly, the sciatic nerves were digested with 0.125% trypsin for 30 min and 1% collagenase for 10 min at 37 °C. The resulting cells were cultured in DMEM medium supplemented with 10% FBS. After 1 h-incubation, the supernatant was discarded and the precipitated cells were cultured in fresh DMEM medium with 10% FBS. Subsequently, the medium was changed every two days with fresh DMEM containing 10% FBS. Cells were passaged when cell confluency reaches 90% and cultured in DMEM

containing 10% exosome-free FBS. Cells of passage 3 were used to prepare exosomes.

4.4. Exosome preparation, characterization and treatment

Primary fibroblasts were plated in coated cell culture dishes at a density of 5×10^7 cells/ml. Fibroblasts were treated with or without 1 mg/ml COS for 6 h, then the supernatants were harvested and subjected to serial centrifugations. Debris and dead cells were removed by centrifugation at 1,000×*g* for 10 min at 4 °C. The resulting solutions were filtrated using 0.22 μm filter and then subjected to ultracentrifugation at 100,000×*g* for 4 h at 4 °C. After washing with PBS, the exosome-containing pellets were resuspended in PBS and allocated and stored in −80 °C freezer until use.

The transmission electron microscope (TEM) was used to identify the morphology of exosomes. Nanoparticle tracking analysis (NTA) was used to measure exosome diameters and particle numbers. Moreover, exosome-specific protein markers CD81 and CD9 were detected by western blot. To monitor exosome internalization in dorsal root ganglion (DRG), exosomes were labeled with PKH26 using a PKH26 fluorescent cell linker kit (Sigma-Aldrich). The labeled exosomes were washed in PBS and collected by ultracentrifugation (100,000×*g* for 20 min) at 4 °C. The resulting PKH26-labeled exosomes were resuspended in PBS and used for internalization assays.

For *in vivo* experiment, SD rats were randomly divided into 3 groups: control group, f-EXOs group, and COS-f-EXOs group (n = 6 per group). The transected sciatic nerves were bridged with silicone tubes filled with exosomes at the dosage of 8.1×10^8 particles/rat. Animals in control group were received saline.

4.5. Dorsal root ganglion culture

Dorsal root ganglion (DRG) was isolated from embryonic (E14) Sprague-Dawley rats. DRG was pulled off with micro forceps and transferred to fresh HBSS medium, where the axon roots and dural tissues were manually removed. The DRG was cultured on Poly-L-Lysine coated plates with Neurobasal medium supplemented with 2% B27, Glutamine (2 mM). The next day, cell culture medium was replaced by Neurobasal medium supplemented with 2% B27, 10 nM uridine, 10 nM 5-fluorodeoxyuridine (FdUr) and 2 mM glutamine. After two days, the cultures were switched to fresh medium without FdUr and uridine mixture. To obtain pure DRG, the above steps could be repeated three times. The medium used above contained 50 ng/ml nerve growth factor (NGF).

DRG neurons were removed from the embryonic (E14) Sprague-Dawley rats, and transferred to fresh HBSS medium, where the axon roots and dural tissue were manually removed. The DRG neurons were then transferred to 0.1% collagenase type I. Following 30 min incubation at 37 °C, the DRG neurons were dissociated in 0.25% trypsin (Gibco) for an additional 10 min at 37 °C, and mechanically triturated through a pipette into the single cell suspension. To remove non-neuron cells, a partial purification step was performed by centrifugation at 1000 rpm for 5 min on 5% fetal bovine serum (FBS) in DMEM solution. The obtained DRG neurons were cultured on coated plates in Neurobasal and B-27 (Gibco) supplemented with 10 nM uridine, 10 nM FdUr, penicillin–streptomycin (both 50 U/ml, Gibco), glutamine (2 mM) and NGF (50 ng/ml). The next day, the cells were purified by 10 μM cytosine arabinoside. After two days, the cultures were switched to fresh medium with penicillin–streptomycin, glutamine and NGF. The pure neurons can be obtained by repeating the steps up to three times.

For neurite outgrowth assay, f-EXOs or COS-f-EXOs were co-cultured with DRG neurons for 24 h, 48 h or 72 h as indicated. NF staining was used to visualize neuronal axons and cell bodies. The lengths of neurites from each DRG neuron were measured by the NeuronJ in the ImageJ software. In each experiment, 8 neurons per condition were selected randomly for neurite outgrowth assay.

4.6. Electroporation

To improve transfection efficiency in cultured DRG neurons, the electroporation instrument (NEPA21, Japan) was employed for this aim. The mimic or inhibitor of miR-132-5p, and the siRNAs for *Tfap2c* and *Camkk1*, were designed and synthesized at RiboBio (Guangzhou, China). The sequences of *Tfap2c* siRNAs are listed in Table S3. For electroporation, 5 nM miR-132-5p mimic or inhibitor, or *Tfap2c* siRNA, or *Camkk1* siRNA mixed with Neurobasal medium (Gibco) were used for *in vitro* transfection. The electroporation was performed using a CUY900-13-3-5 adherent cell electrode (2 times, 50 ms pulses at 20V with 50 ms interval).

4.7. Total RNA isolation from rat plasma extracellular vesicles

Total RNA from rat plasma was isolated and purified by using an exoRNeasySerum/Plasma Midi Kit (QIAGEN, #77064). Briefly, prefiltered plasma was mixed with binding buffer and added to the exoEasy membrane affinity column to bind the EVs to the membrane. After centrifugation, the flow-through was discarded and wash buffer was added to the column to wash off non-specifically retained materials. After 2 time-washing, the vesicles were lysed by adding QIAzol to the spin column, and the lysate was collected by centrifugation. Following addition of chloroform, thorough mixing and centrifugation were performed to separate organic and aqueous phases, and the aqueous phase was collected and mixed with ethanol. The sample-ethanol mixture was added to a RNeasy MinElute spin column and centrifuged. The column was washed once with buffer RWT, and then twice with buffer RPE followed by elution of RNA in water. This procedure allows concentrating the exosome RNA from 1 ml plasma or serum into a final volume of 14 μl of water [70].

4.8. Western blot analysis

Tissues were homogenized with a dounce homogenizer in ice-cold tissue lysis buffer (25 mM Tris-HCl, pH 7.4; 100 mM NaF; 50 mM $Na_4P_2O_7$; 10 mM Na_3VO_4; 10 mM EGTA; 10 mM EDTA; 1% NP-40; 10 μg/ml leupeptin; 10 μg/ml aprotinin; 2 mM PMSF, and 20 nM Okadaic acid) [71]. Cells were lysed in lysis buffer as mentioned above. Exosomal proteins were extracted by using exosomal protein lysis buffer (101Bio). The protein concentration was quantified by using a protein assay kit (Bio-Rad) and normalized with lysis buffer to have equivalent amounts of protein and volume. Protein was denatured by boiling at 100 °C for 5 min in 1X Laemmli buffer. The lysates were cooled to room temperature and resolved by SDS-PAGE and then transferred to polyvinylidene fluoride (PVDF) membrane. After 1-h blocking at room temperature with 10% blocking reagent (Roche), the membrane was incubated overnight with primary antibodies including anti-CD9 (Abcam, ab236630), anti-CD81 (Sigma-Aldrich, SAB3500454), anti-Calnexin (Abcam, ab133615), anti-CAMKK1 (Cell Signaling Technology, #3357), anti-p-Akt (Cell Signaling Technology, 4060), anti-Akt (Cell Signaling Technology, 4685), and anti-Actin (Abcam, ab179467) in Tris-buffered saline solution/Tween (TBST) containing 10% blocking reagent at 4 °C. After the incubation, the membrane was washed three times in TBST and incubated with secondary antibody for 1 h at room temperature. After three-time washing in TBST, the membrane was developed using a chemiluminescence assay system and exposed to Kodak exposure films.

4.9. Quantitative real-time PCR

Total RNA was extracted from cells or animal tissues using the Trizol reagent and transcribed into cDNA by using PrimeScript™ RT Master Mix (Takara). For miRNA detection, mature miRNAs were reversely transcribed with specific Bulge-LoopTM miRNA RT primers using a Bulge-LoopTM miRNA qRT-PCR Starter Kit (RiboBio). The gene

expression analysis was performed with StepOne Real-Time PCR Detection System (Applied Biosystems) with SYBR Green Supermix. The relative expression was calculated by the comparative $2^{-\triangle\triangle Ct}$ method. The mRNA level was normalized to *Gapdh*. Primers used in this study are listed in Table S3.

4.10. Generation of luciferase reporter plasmids and luciferase activity assay

The plasmid of pLVX-Puro-luc was obtained from Miaolingbio (Wuhan, China) and was used to construct the dual luciferase reporter gene system. The four sequences containing predicted TFAP2C binding sites were synthesized and inserted into pLVX-Puro-luc to construct luciferase reporter plasmids. The used sequences are listed in Table S3. To examine the effect of TFAP2C on luciferase activity, HEK293T cells were co-transfected with 200 ng TFAP2C or empty vector (pcDNA3.1; Invitrogen), 200 ng luciferase reporter plasmids, and 25 ng PGL4.74 [hRluc/TK] plasmid (Promega). 24 h post-transfection, cell lysates were prepared and subjected to luciferase activity assay with a commercial kit (Vazyme).

4.11. Immunofluorescence staining

The procedures of immunofluorescence were described elsewhere [21]. Briefly, cells were fixed with pre-cooled 95% ethanol for 30 min; after rehydrating in PBS, the cultures were incubated in blocking solution (10% normal goat serum and 0.03 g/ml BSA) for 1 h at 37 °C followed by incubation with primary antibodies overnight at 4 °C. The next day, after washing three times in PBS, the cultures were incubated with the appropriate secondary antibodies for 1 h at room temperature. The nucleus was labeled with Hoechst for 10 min at room temperature. At the chosen time points post-surgery, rats were sacrificed and the scaffolds, together with nerves, were harvested and cut into sections. Sections were incubated with monoclonal mouse anti-Vimentin (1:200 dilution, Santa Cruz), monoclonal mouse anti-Rab 21 (1:200 dilution, Santa Cruz), polyclonal rabbit anti-Rtn3 (1:150 dilution, Proteintech), monoclonal rabbit anti-CD68 antibody (1:200 dilution, Abcam), polyclonal rabbit anti-S100 antibody (1:200, dilution), monoclonal mouse anti-NF antibody (1:200 dilution), and mouse anti-S100 antibody (1:200 dilution) at 4 °C for 36 h. The sections were further reacted with the FITC-labeled secondary antibody goat anti-mouse IgG (1:400 dilution), or the Cy3-labeled secondary antibody sheep anti rabbit IgG (1:400 dilution) at 4 °C overnight, followed by observation under a confocal laser scanning microscope (Leica, Heidelberg, Germany).

4.12. Behavioral tests

The gait analysis system was performed to assess function recovery of rats after nerve grafting. Pre-training was given 2 weeks before surgery. Animals were allowed to walk along a glass platform, underneath which each run was captured by a video camera. The outcome parameters include maximum contact area, stride length, and swing speed. Data were collected and analyzed with the CatWalk software (CatWalk XT Version 10.5), and mean intensity and sciatic function index (SFI) value was calculated by the formula based on the method of others [72]. 12 weeks after grafting, compound muscle action potential (CMAP) was measured, and the motor nerve conduction (MCV) was calculated with the method described previously [73]. Briefly, the sciatic nerves at the experimental sides were re-exposed under anesthesia. The recording electrode was accurately inserted into the muscled abdomen of the gastrocnemius muscle. Then electric stimulation with 5.0 mA and 0.1 ms pulse width was applied to the distal and proximal parts of the sciatic nerve, respectively. The CMAP and latency were recorded, and the MCV was calculated.

4.13. Statistical analysis

The statistical significance was analyzed by GraphPad Prism 8.0 (GraphPad Software, Inc.). Student's *t*-test was used to calculate significance between two groups. One-way analysis of variance (ANOVA) followed by Bonferroni's Multiple Comparison test, or two-way ANOVA followed by Sidak multiple comparisons test was employed for analyzing statistical difference in multiple groups. Data were presented as mean ± SD. $P < 0.05$ was considered statistically significant.

Ethics approval and consent to participate

The study received approval from the institutional review board of Nantong University.

Data availability

All data reported in this study are present in the paper or the Supplementary information. All relevant data are available from the corresponding authors.

CRediT authorship contribution statement

Yahong Zhao: Formal analysis, Methodology, Resources, Writing - original draft, Writing - review & editing. **Jina Liu:** Project administration, Validation, Visualization. **Sha Liu:** Formal analysis, Data curation. **Panpan Yang:** Project administration, Validation. **Yunyun Liang:** Formal analysis, Data curation. **Jinyu Ma:** Investigation, Project administration. **Susu Mao:** Methodology, Software. **Cheng Sun:** Supervision, Conceptualization, Writing - original draft, Writing - review & editing. **Yumin Yang:** Supervision, Conceptualization, Funding acquisition, Writing - review & editing.

Declaration of competing interest

The authors declare no conflict of interests.

Acknowledgements

The present study was financially supported by the National Natural Science Foundation of China (Nos. 32230057; 81970747; 32271193); the National Key Research and Development Program of China (No. 2017YFA0701304); the Priority Academic Program Development (PAPD) of Jiangsu Higher Education Institutions.

Appendix A. Supplementary data

Supplementary data to this article can be found online at https://doi.org/10.1016/j.bioactmat.2023.03.002.

References

[1] Z. He, Y. Jin, Intrinsic control of axon regeneration, Neuron 90 (2016) 437–451, https://doi.org/10.1016/j.neuron.2016.04.022.
[2] M. Mahar, V. Cavalli, Intrinsic mechanisms of neuronal axon regeneration, Nat. Rev. Neurosci. 19 (2018) 323–337, https://doi.org/10.1038/s41583-018-0001-8.
[3] A. Tedeschi, F. Bradke, Spatial and temporal arrangement of neuronal intrinsic and extrinsic mechanisms controlling axon regeneration, Curr. Opin. Neurobiol. 42 (2017) 118–127, https://doi.org/10.1016/j.conb.2016.12.005.
[4] S.K. Lee, S.W. Wolfe, Peripheral nerve injury and repair, J. Am. Acad. Orthop. Surg. 8 (2000) 243–252, https://doi.org/10.5435/00124635-200007000-00005.
[5] H. Millesi, Techniques for nerve grafting, Hand Clin. 16 (2000) 73–91, viii.
[6] X. Gu, F. Ding, D.F. Williams, Neural tissue engineering options for peripheral nerve regeneration, Biomaterials 35 (2014) 6143–6156, https://doi.org/10.1016/j.biomaterials.2014.04.064.
[7] X. Gu, F. Ding, Y. Yang, J. Liu, Construction of tissue engineered nerve grafts and their application in peripheral nerve regeneration, Prog. Neurobiol. 93 (2011) 204–230, https://doi.org/10.1016/j.pneurobio.2010.11.002.

[8] S. Vijayavenkataraman, Nerve guide conduits for peripheral nerve injury repair: a review on design, materials and fabrication methods, Acta Biomater. 106 (2020) 54–69, https://doi.org/10.1016/j.actbio.2020.02.003.

[9] B. Gong, et al., Neural tissue engineering: from bioactive scaffolds and in situ monitoring to regeneration, Explorations 2 (2022), https://doi.org/10.1002/exp.20210035.

[10] N.U. Kang, S.J. Lee, S.J. Gwak, Fabrication techniques of nerve guidance conduits for nerve regeneration, Yonsei Med. J. 63 (2022) 114–123, https://doi.org/10.3349/ymj.2022.63.2.114.

[11] L.F. Li, et al., Electrospun fibers control drug delivery for tissue regeneration and cancer therapy, Adv Fiber Mater (2022), https://doi.org/10.1007/s42765-022-00198-9.

[12] Y. Fang, et al., 3D printed conductive multiscale nerve guidance conduit with hierarchical fibers for peripheral nerve regeneration, Adv. Sci. (2023), e2205744, https://doi.org/10.1002/advs.202205744.

[13] S. Rashki, et al., Chitosan-based nanoparticles against bacterial infections, Carbohydr. Polym. 251 (2021), 117108, https://doi.org/10.1016/j.carbpol.2020.117108.

[14] K.R. Shoueir, et al., Chitosan based-nanoparticles and nanocapsules: overview, physicochemical features, applications of a nanofibrous scaffold, and bioprinting, Int. J. Biol. Macromol. (2020), https://doi.org/10.1016/j.ijbiomac.2020.11.072.

[15] C. Xue, et al., Joint use of a chitosan/PLGA scaffold and MSCs to bridge an extra large gap in dog sciatic nerve, Neurorehabilitation Neural Repair 26 (2012) 96–106, https://doi.org/10.1177/1545968311420444.

[16] N. Hu, et al., Long-term outcome of the repair of 50 mm long median nerve defects in rhesus monkeys with marrow mesenchymal stem cells-containing, chitosan-based tissue engineered nerve grafts, Biomaterials 34 (2013) 100–111, https://doi.org/10.1016/j.biomaterials.2012.09.020.

[17] Y. Gu, et al., Chitosan/silk fibroin-based, Schwann cell-derived extracellular matrix-modified scaffolds for bridging rat sciatic nerve gaps, Biomaterials 35 (2014) 2253–2263, https://doi.org/10.1016/j.biomaterials.2013.11.087.

[18] H. Wang, et al., Repairing rat sciatic nerve injury by a nerve-growth-factor-loaded, chitosan-based nerve conduit, Biotechnol. Appl. Biochem. 59 (2012) 388–394, https://doi.org/10.1002/bab.1031.

[19] W. Fan, et al., Repairing a 35-mm-long median nerve defect with a chitosan/PGA artificial nerve graft in the human: a case study, Microsurgery 28 (2008) 238–242, https://doi.org/10.1002/micr.20488.

[20] Y. Wang, et al., Chitosan degradation products promote nerve regeneration by stimulating Schwann cell proliferation via miR-27a/FOXO1 Axis, Mol. Neurobiol. 53 (2016) 28–39, https://doi.org/10.1007/s12035-014-8968-2.

[21] Y. Zhao, et al., Chitosan degradation products facilitate peripheral nerve regeneration by improving macrophage-constructed microenvironments, Biomaterials 134 (2017) 64–77, https://doi.org/10.1016/j.biomaterials.2017.02.026.

[22] R. Kalluri, V.S. LeBleu, The biology, function, and biomedical applications of exosomes, Science 367 (2020), https://doi.org/10.1126/science.aau6977.

[23] X. Zhou, et al., Exosome-mediated crosstalk between keratinocytes and macrophages in cutaneous wound healing, ACS Nano 14 (2020) 12732–12748, https://doi.org/10.1021/acsnano.0c03064.

[24] W. Ying, et al., Adipose tissue macrophage-derived exosomal miRNAs can modulate in vivo and in vitro insulin sensitivity, Cell 171 (2017) 372–384 e312, https://doi.org/10.1016/j.cell.2017.08.035.

[25] Y. Xie, et al., Involvement of serum-derived exosomes of elderly patients with bone loss in failure of bone remodeling via alteration of exosomal bone-related proteins, Aging Cell 17 (2018), e12758, https://doi.org/10.1111/acel.12758.

[26] A. Hoshino, et al., Extracellular vesicle and particle biomarkers define multiple human cancers, Cell 182 (2020) 1044–1061 e1018, https://doi.org/10.1016/j.cell.2020.07.009.

[27] Y. Wang, et al., Involvement of macrophage-derived exosomes in abdominal aortic aneurysms development, Atherosclerosis 289 (2019) 64–72, https://doi.org/10.1016/j.atherosclerosis.2019.08.016.

[28] M. Guo, et al., Microglial exosomes facilitate alpha-synuclein transmission in Parkinson's disease, Brain : J. Neurol. 143 (2020) 1476–1497, https://doi.org/10.1093/brain/awaa090.

[29] Y. Sun, et al., Human mesenchymal stem cell derived exosomes alleviate type 2 diabetes mellitus by reversing peripheral insulin resistance and relieving beta-cell destruction, ACS Nano 12 (2018) 7613–7628, https://doi.org/10.1021/acsnano.7b07643.

[30] Z.W. Luo, et al., Aptamer-functionalized exosomes from bone marrow stromal cells target bone to promote bone regeneration, Nanoscale 11 (2019) 20884–20892, https://doi.org/10.1039/c9nr02791b.

[31] S. Kamerkar, et al., Exosomes facilitate therapeutic targeting of oncogenic KRAS in pancreatic cancer, Nature 546 (2017) 498–503, https://doi.org/10.1038/nature22341.

[32] L. Bouchareychas, et al., Macrophage exosomes resolve atherosclerosis by regulating hematopoiesis and inflammation via MicroRNA cargo, Cell Rep. 32 (2020), 107881, https://doi.org/10.1016/j.celrep.2020.107881.

[33] M. Izco, et al., Systemic exosomal delivery of shRNA minicircles prevents parkinsonian pathology, Mol. Ther. : the journal of the American Society of Gene Therapy 27 (2019) 2111–2122, https://doi.org/10.1016/j.ymthe.2019.08.010.

[34] G. Wu, et al., Molecularly engineered macrophage-derived exosomes with inflammation tropism and intrinsic heme biosynthesis for atherosclerosis treatment, Angew. Chem. 59 (2020) 4068–4074, https://doi.org/10.1002/anie.201913700.

[35] Z.L. Chen, W.M. Yu, S. Strickland, Peripheral regeneration, Annu. Rev. Neurosci. 30 (2007) 209–233, https://doi.org/10.1146/annurev.neuro.30.051606.094337.

[36] J.A. Pereira, F. Lebrun-Julien, U. Suter, Molecular mechanisms regulating myelination in the peripheral nervous system, Trends Neurosci. 35 (2012) 123–134, https://doi.org/10.1016/j.tins.2011.11.006.

[37] Y. Zhao, et al., Exosomal miR-673-5p from fibroblasts promotes Schwann cell-mediated peripheral neuron myelination by targeting the TSC2/mTORC1/SREBP2 axis, J. Biol. Chem. 298 (2022), 101718, https://doi.org/10.1016/j.jbc.2022.101718.

[38] W.A. Pastor, et al., TFAP2C regulates transcription in human naive pluripotency by opening enhancers, Nat. Cell Biol. 20 (2018) 553–564, https://doi.org/10.1038/s41556-018-0089-0.

[39] D. Chen, et al., The TFAP2C-regulated OCT4 naive enhancer is involved in human germline formation, Cell Rep. 25 (2018) 3591–3602 e3595, https://doi.org/10.1016/j.celrep.2018.12.011.

[40] A.R. Cyr, et al., TFAP2C governs the luminal epithelial phenotype in mammary development and carcinogenesis, Oncogene 34 (2015) 436–444, https://doi.org/10.1038/onc.2013.569.

[41] L. Li, et al., TFAP2C- and p63-dependent networks sequentially rearrange chromatin landscapes to drive human epidermal lineage commitment, Cell Stem Cell 24 (2019) 271–284 e278, https://doi.org/10.1016/j.stem.2018.12.012.

[42] D. Park, et al., Extracellular matrix anisotropy is determined by TFAP2C-dependent regulation of cell collisions, Nat. Mater. 19 (2020) 227–238, https://doi.org/10.1038/s41563-019-0504-3.

[43] R. Lopes, et al., Systematic dissection of transcriptional regulatory networks by genome-scale and single-cell CRISPR screens, Sci. Adv. 7 (2021), https://doi.org/10.1126/sciadv.abf5733.

[44] M. Zhu, et al., Developmental clock and mechanism of de novo polarization of the mouse embryo, Science 370 (2020), https://doi.org/10.1126/science.abd2703.

[45] A. Mateus-Pinheiro, et al., AP2gamma controls adult hippocampal neurogenesis and modulates cognitive, but not anxiety or depressive-like behavior, Mol. Psychiatr. 22 (2017) 1725–1734, https://doi.org/10.1038/mp.2016.169.

[46] D. Eckert, S. Buhl, S. Weber, R. Jager, H. Schorle, The AP-2 family of transcription factors, Genome Biol. 6 (2005) 246, https://doi.org/10.1186/gb-2005-6-13-246.

[47] M. Kokubo, et al., BDNF-mediated cerebellar granule cell development is impaired in mice null for CaMKK2 or CaMKIV, J. Neurosci. 29 (2009) 8901–8913, https://doi.org/10.1523/JNEUROSCI.0040-09.2009.

[48] H. Jiao, et al., Chitosan/polyglycolic acid nerve grafts for axon regeneration from prolonged axotomized neurons to chronically denervated segments, Biomaterials 30 (2009) 5004–5018, https://doi.org/10.1016/j.biomaterials.2009.05.059.

[49] Y. Gong, L. Gong, X. Gu, F. Ding, Chitooligosaccharides promote peripheral nerve regeneration in a rabbit common peroneal nerve crush injury model, Microsurgery 29 (2009) 650–656, https://doi.org/10.1002/micr.20686.

[50] P.K. Thomas, The connective tissue of peripheral nerve: an electron microscope study, J. Anat. 97 (1963) 35–44.

[51] S. Mahmoudi, et al., Heterogeneity in old fibroblasts is linked to variability in reprogramming and wound healing, Nature 574 (2019) 553–558, https://doi.org/10.1038/s41586-019-1658-5.

[52] M.V. Plikus, et al., Regeneration of fat cells from myofibroblasts during wound healing, Science 355 (2017) 748–752, https://doi.org/10.1126/science.aai8792.

[53] M.D. Tallquist, J.D. Molkentin, Redefining the identity of cardiac fibroblasts, Nat. Rev. Cardiol. 14 (2017) 484–491, https://doi.org/10.1038/nrcardio.2017.57.

[54] L. Moretti, J. Stalfort, T.H. Barker, D. Abebayehu, The interplay of fibroblasts, the extracellular matrix, and inflammation in scar formation, J. Biol. Chem. 298 (2022), 101530, https://doi.org/10.1016/j.jbc.2021.101530.

[55] X. Chen, E. Song, Turning foes to friends: targeting cancer-associated fibroblasts, Nat. Rev. Drug Discov. 18 (2019) 99–115, https://doi.org/10.1038/s41573-018-0004-1.

[56] M.V. Plikus, et al., Fibroblasts: origins, definitions, and functions in health and disease, Cell 184 (2021) 3852–3872, https://doi.org/10.1016/j.cell.2021.06.024.

[57] S. Wankhade, Y. Yu, J. Weinberg, M.A. Tainsky, P. Kannan, Characterization of the activation domains of AP-2 family transcription factors, J. Biol. Chem. 275 (2000) 29701–29708, https://doi.org/10.1074/jbc.M000931200.

[58] P.P. Wong, et al., Histone demethylase KDM5B collaborates with TFAP2C and Myc to repress the cell cycle inhibitor p21(cip) (CDKN1A), Mol. Cell Biol. 32 (2012) 1633–1644, https://doi.org/10.1128/MCB.06373-11.

[59] D. Jean, et al., Loss of AP-2 results in up-regulation of MCAM/MUC18 and an increase in tumor growth and metastasis of human melanoma cells, J. Biol. Chem. 273 (1998) 16501–16508, https://doi.org/10.1074/jbc.273.26.16501.

[60] S. Gaubatz, et al., Transcriptional activation by Myc is under negative control by the transcription factor AP-2, EMBO J. 14 (1995) 1508–1519, https://doi.org/10.1002/j.1460-2075.1995.tb07137.x.

[61] C. Wang, et al., Increased level of exosomal miR-20b-5p derived from hypothermia-treated microglia promotes neurite outgrowth and synapse recovery after traumatic brain injury, Neurobiol. Dis. 179 (2023), 106042, https://doi.org/10.1016/j.nbd.2023.106042.

[62] H. Xin, et al., Exosome-mediated transfer of miR-133b from multipotent mesenchymal stromal cells to neural cells contributes to neurite outgrowth, Stem Cell. 30 (2012) 1556–1564, https://doi.org/10.1002/stem.1129.

[63] G.A. Wayman, et al., Regulation of axonal extension and growth cone motility by calmodulin-dependent protein kinase I, J. Neurosci. 24 (2004) 3786–3794, https://doi.org/10.1523/JNEUROSCI.3294-03.2004.

[64] N.V. Uboha, M. Flajolet, A.C. Nairn, M.R. Picciotto, A calcium- and calmodulin-dependent kinase Ialpha/microtubule affinity regulating kinase 2 signaling cascade mediates calcium-dependent neurite outgrowth, J. Neurosci. 27 (2007) 4413–4423, https://doi.org/10.1523/JNEUROSCI.0725-07.2007.

[65] N. Ageta-Ishihara, et al., Control of cortical axon elongation by a GABA-driven Ca2+/calmodulin-dependent protein kinase cascade, J. Neurosci. 29 (2009) 13720–13729, https://doi.org/10.1523/JNEUROSCI.3018-09.2009.
[66] Y. Tai, et al., TRPC6 channels promote dendritic growth via the CaMKIV-CREB pathway, J. Cell Sci. 121 (2008) 2301–2307, https://doi.org/10.1242/jcs.026906.
[67] J.H. Heiser, et al., TRPC6 channel-mediated neurite outgrowth in PC12 cells and hippocampal neurons involves activation of RAS/MEK/ERK, PI3K, and CAMKIV signaling, J. Neurochem. 127 (2013) 303–313, https://doi.org/10.1111/jnc.12376.
[68] X. Wu, E. Xiong, W. Wang, M. Scali, M. Cresti, Universal sample preparation method integrating trichloroacetic acid/acetone precipitation with phenol extraction for crop proteomic analysis, Nat. Protoc. 9 (2014) 362–374, https://doi.org/10.1038/nprot.2014.022.
[69] P. Shannon, et al., Cytoscape: a software environment for integrated models of biomolecular interaction networks, Genome Res. 13 (2003) 2498–2504, https://doi.org/10.1101/gr.1239303.
[70] D. Enderle, et al., Characterization of RNA from exosomes and other extracellular vesicles isolated by a novel spin column-based method, PLoS One 10 (2015), e0136133, https://doi.org/10.1371/journal.pone.0136133.
[71] C. Sun, et al., PCAF improves glucose homeostasis by suppressing the gluconeogenic activity of PGC-1alpha, Cell Rep. 9 (2014) 2250–2262, https://doi.org/10.1016/j.celrep.2014.11.029.
[72] E.A. Kappos, et al., Validity and reliability of the CatWalk system as a static and dynamic gait analysis tool for the assessment of functional nerve recovery in small animal models, Brain Behav 7 (2017), e00723, https://doi.org/10.1002/brb3.723.
[73] L. Zhang, et al., Genipin-cross-linked chitosan nerve conduits containing TNF-alpha inhibitors for peripheral nerve repair, Ann. Biomed. Eng. 46 (2018) 1013–1025, https://doi.org/10.1007/s10439-018-2011-0.